Hybrid system for in vivo epifluorescence and 4D optoacoustic imaging

Chen, Zhenyue ; Deán-Ben, Xosé Luis ; Gottschalk, Sven ; Razansky, Daniel

Abstract: Epifluorescence imaging is widely used in cell and molecular biology due to its excellent sensitivity, contrast, and ease of implementation. Optoacoustic imaging has been shown to deliver a highly complementary and unique set of capabilities for biological discovery, such as high spatial resolution in noninvasive deep tissue observations, fast volumetric imaging capacity, and spectrally enriched contrast. In this Letter, we report on a hybrid system combining planar fluorescence and real-time volumetric four-dimensional optoacoustic imaging by means of a fiberscope integrated within a handheld hemispherical ultrasound detection array. The in vivo imaging performance is demonstrated by non-invasive visualization of fast contrast agent perfusion through the mouse brain. The proposed synergistic combination of fluorescence and optoacoustic imaging can benefit numerous studies looking at multi-scale in vivo dynamics, such as functional neuroimaging, visualization of organ perfusion and contrast agent uptake, cell tracking, and pharmacokinetic and bio-distribution analysis.

DOI: https://doi.org/10.1364/ol.42.004577

Optics Letters

Hybrid system for in vivo epifluorescence and 4D optoacoustic imaging

Zhenyue Chen,[1,2] Xosé Luis Deán-Ben,[2] Sven Gottschalk,[2] and Daniel Razansky[1,2,*]

[1]Faculty of Medicine, Technical University of Munich, Ismaninger Str. 22, 81675 Munich, Germany
[2]Institute for Biological and Medical Imaging (IBMI), Helmholtz Center Munich, Ingolstädter Landstr. 1, 85764 Neuherberg, Germany
*Corresponding author: dr@tum.de

Received 8 August 2017; revised 4 October 2017; accepted 7 October 2017; posted 9 October 2017 (Doc. ID 303932); published 0 MONTH 0000

Epifluorescence imaging is widely used in cell and molecular biology due to its excellent sensitivity, contrast, and ease of implementation. Optoacoustic imaging has been shown to deliver a highly complementary and unique set of capabilities for biological discovery, such as high spatial resolution in noninvasive deep tissue observations, fast volumetric imaging capacity, and spectrally enriched contrast. In this Letter, we report on a hybrid system combining planar fluorescence and real-time volumetric four-dimensional optoacoustic imaging by means of a fiberscope integrated within a handheld hemispherical ultrasound detection array. The *in vivo* imaging performance is demonstrated by noninvasive visualization of fast contrast agent perfusion through the mouse brain. The proposed synergistic combination of fluorescence and optoacoustic imaging can benefit numerous studies looking at multi-scale *in vivo* dynamics, such as functional neuroimaging, visualization of organ perfusion and contrast agent uptake, cell tracking, and pharmacokinetic and bio-distribution analysis.

OCIS codes: (110.0110) Imaging systems; (170.0170) Medical optics and biotechnology; (110.5120) Photoacoustic imaging; (110.6880) Three-dimensional image acquisition; (170.5120) Photoacoustic imaging; (170.2520) Fluorescence microscopy.

https://doi.org/10.1364/OL.99.099999

Fluorescence imaging is a powerful approach for the dynamic visualization of anatomy and function in biological tissues with high specificity. A myriad of existing fluorescent compounds (fluorophores) enable to specifically label molecular targets in cellular and subcellular structures and, hence, provide experimental observations of gene expression and other molecular pathways in health and disease [1]. At the cellular level, state-of-the-art fluorescence microscopes can also overcome the spatial resolution limit imposed by optical diffraction [2] or provide sufficient temporal resolution to capture changes in fluorescent indicators of neural activity [3]. However, fluorescence microscopy is inherently constrained by light scattering, which limits the reachable depth to ~1 mm in diffuse tissues. At macroscopic scales, fluorescent probes with excitation and emission spectra in the near-infrared (NIR) spectral window may still enable retrieving molecular information from deep tissues [4,5], albeit with poor spatial resolution governed by the diffusive propagation regime of light [6]. Macroscopic epifluorescence imaging in the visible region has found many useful applications, such as monitoring of neuronal activity with calcium or voltage indicators [7,8], while the availability of high-sensitivity cameras in a second NIR window in combination with newly developed fluorescent probes can significantly enhance the imaging depth [9].

In contrast to tomographic imaging methods based on diffuse optics, optoacoustic (OA) imaging is known to deliver a unique set of capabilities that stem from the higher spatial and temporal resolution of ultrasound-based image formation approaches. OA imaging further provides deep penetration, resolution scalability from microscopic to macroscopic dimensions, and spectrally enriched imaging contrast [10–13]. State-of-the-art OA systems have been shown to provide five-dimensional imaging capacity by simultaneously delivering spectrally resolved information three-dimensionally and in real time [14]. The label-free optical absorption contrast exploited in biomedical OA imaging readily enables detecting the presence of intrinsic tissue components, such as oxy- and deoxyhemoglobin, melanin, bilirubin, lipids, and water [15]. Importantly, the inherent spectral sensitivity of multi-spectral OA imaging has enabled sensitive differentiation of many organic fluorescent dyes. Dyes with peak absorption at NIR wavelengths, such as indocyanine green (ICG) [16], are particularly suitable for deep tissue OA imaging due to their high extinction coefficient and a relatively low quantum yield [17].

To this end, a number of approaches have been suggested for combining fluorescence and OA measurements. For example, OA tomography (OAT) and fluorescence molecular tomography have been combined and compared [18]. Two separate OA and planar fluorescence systems have also been hybridized [19,20]. Dual-modality microscopes for superficial imaging applications have further been constructed [21,22]. However, all these approaches were not suitable for simultaneous deep-tissue imaging in both fluorescence and OA modes, while the relatively slow acquisition further hindered the efficient acquisition of dynamic *in vivo* phenomena. Efficient hybridization is also hampered by the limited accessibility of

the imaged area when attempting to collect high-quality data in both fluorescence and OA modes, the latter also necessitating liquid acoustic coupling and large tomographic coverage for optimal three-dimensional (3D) image quality [23]. In this Letter, we present a hybrid system based on the integration of a specifically designed (~~EMCCD~~) fluorescence fiberscope into a spherical ultrasound array optimized for four-dimensional (4D or real-time 3D) OA imaging performance. In this way, both fluorescence and OA responses are excited with the same nanosecond-duration laser pulse guided via optical fibers integrated into the fiberscope, which allows effectively exploiting the contrast mechanisms of both imaging modalities.

A layout of the suggested hybrid imaging system is depicted in Fig. 1. Basically, it consists of a custom-made ~~EMCCD~~ electron multiplying charge-coupled device (EMCCD) based fiberscope for epifluorescence imaging and a hemispherical transducer array for volumetric OA imaging. The transducer array consists of 512 piezocomposite elements disposed on a spherical surface with 40 mm radius covering an angle of 140°. The ultrasound sensing elements have 2.5 mm diameter, 5 MHz central frequency, and ~100% bandwidth (at −6 dB). The distribution of elements guarantees good sensitivity in a region of interest (ROI) around the center of the sphere. The fiberscope is composed of a fiber optic image guide and optical relay system, an illumination fiber bundle, and a high-performance air-cooled EMCCD camera. The scope shaft (custom-made by Zibra Corporation, U.S.) integrates a 1.4 mm fiber optic image guide composed of 100,000 fibers (inset A in Fig. 1), along with an illumination bundle composed of seven silica fibers with 600 μm diameter and 0.4 numerical aperture (insets B and C in Fig. 1). The ultrasound array features a central 8 mm cylindrical opening that matches the outer diameter of the scope's shaft (inset D in Fig. 1). The small diameter of the opening does not significantly affect the effective angular coverage of the spherical array, so that limited view effects in the reconstructed OA images are minimized. The EMCCD camera (Andor Luca R, Oxford Instruments) has an active image area of ~9 × 9 mm, corresponding to 1004 × 1002 pixels with size 8 μm x8 μm. It has a high spectral sensitivity at visible and NIR wavelengths with extremely low noise. An emission filter is placed in front of the camera to selectively filter the fluorescence signals. The illumination bundle was specifically arranged to provide approximately uniform illumination at the center of the array with sufficient energy density to effectively excite both fluorescence and OA responses. Specifically, a short-pulsed (~6 ns duration) wavelength-tunable optical parametric oscillator (OPO) laser (InnoLas Laser GmbH, Germany) was used for the excitation. The ultrasound waves generated by the absorption of each laser pulse in the tissue were collected by the 512 individual detection elements of the spherical array, simultaneously sampled at 40 megasamples per second with a custom-made data acquisition system (Falkenstein Mikrosysteme GmbH, Germany) and transmitted in real time to a PC workstation for volumetric image reconstruction. At the same time, the fluorescence responses acquired by the fiberscope were also transmitted in real time to the PC workstation for display and data analysis.

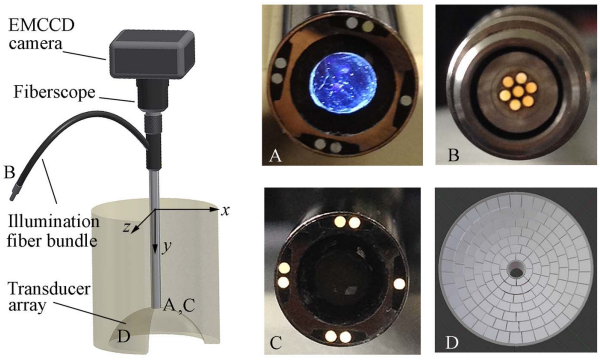

F1:1 F1:2 F1:3 F1:4 **Fig. 1.** Layout of the hybrid planar fluorescence system. Photographs of the imaging bundle, input, and output ends of the illumination bundle and schematic drawing of the transducer array are shown in insets A, B, C, and D.

First, we tested the spatial resolution of the hybrid system. For this, a USAF 1951 test target (Thorlabs R3L3S1N) was placed ~37 mm away from the tip of the scope shaft, corresponding to its standard working distance. White light was coupled into the illumination bundle of the fiberscope. Bandpass optical filters with 525 nm (±19.5 nm, Thorlabs MF525-39) and 800 nm (±20 nm, Andover 800FS40-25) were successively placed in front of the camera, and the corresponding images were acquired. A third acquisition was further performed after removing the filters. The same USAF target was used to evaluate the OA resolution in the lateral x–y plane. It was placed at approximately the center of the spherical array geometry and excited with the OPO laser tuned to 700 nm. The excitation laser beam was coupled into the illumination fiber bundle. No signal averaging was performed for the OA data acquisition. The USAF target was also used to calibrate the azimuthal orientation of the epifluorescence and optoacoustic imaging systems by registering fiducial markers in the images.

Results of the resolution characterization experiments are presented in Fig. 2. Images of the entire USAF target acquired through the 525 nm bandpass filter and its zoom-in are shown in Figs. 2(a) and 2(b), respectively. The corresponding images for the 800 nm wavelength and white light illumination are further displayed in Figs. 2(c) and 2(d). The indicated line profiles allow identifying the thinner lines that can be resolved. The resolution achieved when no filter was used (white light) was approximately 20.16 lp/mm (group 4, element 3), while resolutions of 22.62 lp/mm (group 4, element 4) and 12.7 lp/mm (group 3 element 5) were rendered for the 525 and 800 nm excitation wavelengths, respectively. The inferior resolution at 800 nm is attributed to crosstalk between the individual fibers of the optic image guide at this wavelength range. Figure 2(e) shows the cross section of the OA image of the USAF target. A line profile is also displayed, indicating an approximate resolution of 5.66 lp/mm (group 2, element 4) in the x and y directions. This corresponds to the spatial resolution of 177 μm, in good agreement with the ~5 MHz detection bandwidth of the transducer elements. The table in Fig. 2(f) summarizes the spatial resolution characterization results of the hybrid system.

The synergetic advantages of the real-time hybrid imaging system were subsequently showcased by imaging two 64-day-old athymic nude-Fox1^{nu} mice *in vivo* (Harlan Laboratories LTD, Switzerland). In particular, the brain was imaged following a tail vein injection of 100 μl of ICG at a concentration of 750 μg/ml (~1 mM). The mice were anesthetized with 1–2% isoflurane in oxygen at 0.7–0.8 l/ min. Imaging was performed

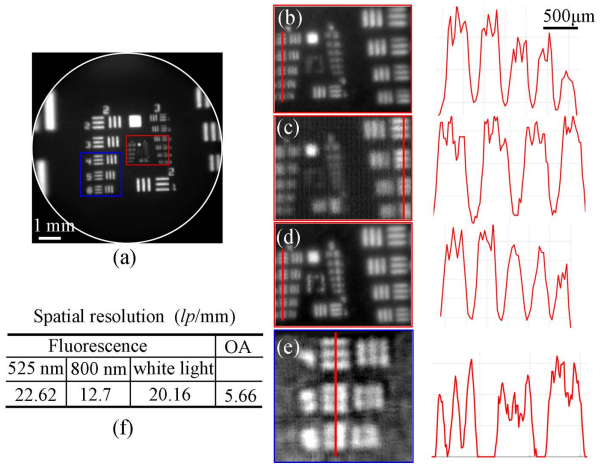

F2:1 **Fig. 2.** Spatial resolution characterization of the hybrid system.
F2:2 (a) Image of the entire USAF 1951 target acquired with the
F2:3 525 nm bandpass filter. The white circle shows the effective FOV
F2:4 of the fiberscope. (b)–(d) show the zoomed-in images acquired for
F2:5 525 nm, 800 nm, white light illumination, and the corresponding
F2:6 1D profiles along the red lines. The imaged area is indicated by
F2:7 the red box in (a). (e) Optoacoustic image acquired from the
F2:8 USAF 1951 target. A single cross section corresponding to the area
F2:9 indicated by a blue box in (a) is shown. (f) Summary table of the mea-
F2:10 sured spatial resolution of the hybrid system.

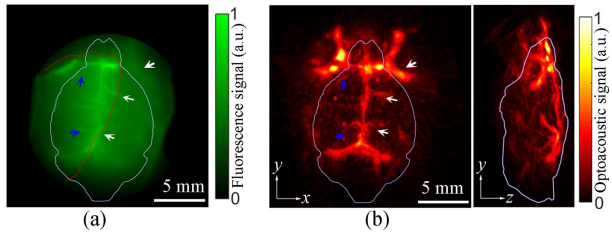

F3:1 **Fig. 3.** Contrast-enhanced imaging of the mouse brain *in vivo*.
F3:2 (a) Fluorescence image of the mouse brain after tail-vein injection
F3:3 of ICG. The red curve shows the boundary of the removed scalp.
F3:4 (b) Corresponding volumetric OA images (maximal intensity projec-
F3:5 tions along z and x axes are shown). The blue arrows show vessels that
F3:6 can be observed in both modalities, while the white arrows show the
F3:7 vessels that can only be clearly observed in the OA images.

193 transcranially, but the scalp was partially removed to evaluate
194 how it affects the imaging performance in both modalities.
195 Animal handling and surgical procedures were performed ac-
196 cording to the directives on animal experimentation of the
197 Helmholtz Zentrum München and with approval from the
198 Government District of Upper Bavaria. The laser was running
199 at a pulse repetition rate of 25 Hz at 700 nm wavelength. The
200 camera integration time was set to 0.1 s. A long pass filter
201 (Edmund Optics, Stock # 66-227) with an 800 nm cut-on
202 wavelength was placed in front of the camera. Time-lapse fluo-
203 rescence and 3D OA data were acquired for a total duration of
204 300 s, starting ~10 s prior to the ICG injection. Following data
205 acquisition, volumetric OAT image reconstruction was done
206 with the 3D filtered back-projection formula [24]. To show
207 the signal variation over time, both fluorescence and OA images
208 were normalized to their corresponding global maxima within
209 the entire recording period.

210 Figure 3 shows the hybrid fluorescence and OA images
211 acquired from the first mouse after the ICG injection. It
212 can readily be seen that the presence of the scalp causes signifi-
213 cant blurring of the underlying vasculature in the fluorescence
214 images, whereas some superficial cortical microvasculature can
215 be more clearly observed when the scalp is removed. In con-
216 trast, no deterioration of image quality is observed in the
217 OA images shown in Fig. 3(b), and all the major vessels are
218 clearly observed under both areas with an intact scalp (indicated
219 by the white arrows) and with the scalp removed (indicated by
220 the blue arrows). Thus, clearly resolvable 3D information can
221 be obtained from deep seated vascular structures way beyond
222 the limits of ballistic light penetration.

223 Figure 4 shows the time lapse imaging results acquired from
224 the second mouse after the ICG injection. Figure 4(a) shows
225 the fluorescence images captured at different time instances,

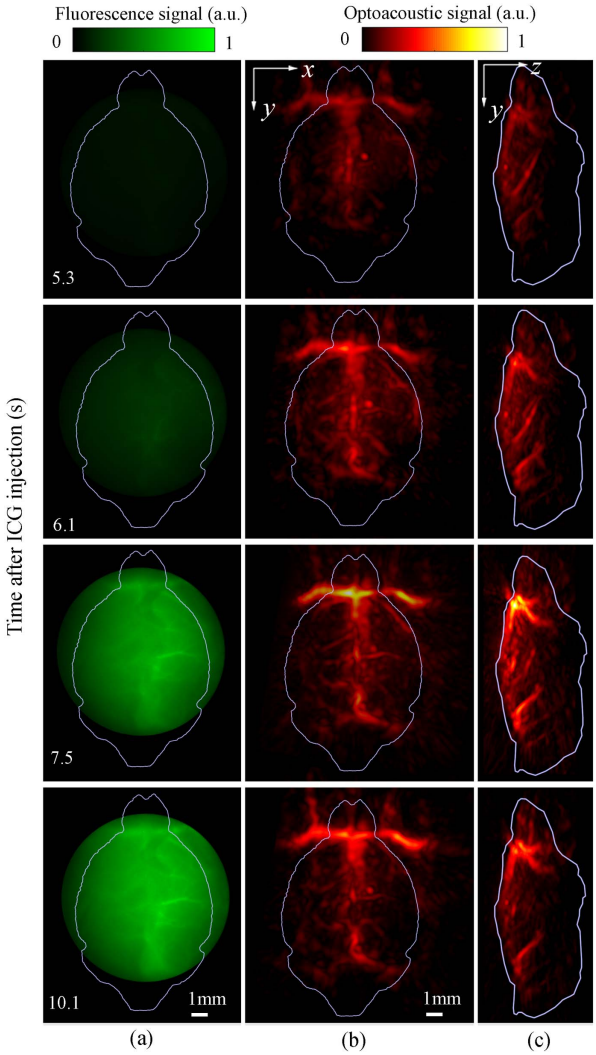

F4:1 **Fig. 4.** Non-invasive time lapse imaging of the mouse brain *in vivo*
F4:2 following ICG injection at $t = 0$. (a) Series of the epifluorescence im-
F4:3 ages. (b) and (c) Corresponding volumetric optoacoustic images; the
F4:4 ~~maximal~~ maximum intensity projections along the depth (z) and lateral (x) axes
F4:5 are shown respectively.

and Fig. 4(b) shows the corresponding optoacoustic images in the x–y and y–z planes. Within a short time following the ICG injection, both fluorescent and OA signals raise sharply. However, the average fluorescent signal level remains at its highest level at 10 s post-injection, while the OA signal starts decreasing after reaching its peak around the 7.5 s time point. This can be attributed to the lack of depth resolving capability of fluorescence with its surface-weighted signal averaged across different depths (see also Visualization 1).

To this end, various implementations of OA imaging and OAT have demonstrated powerful performance in visualizing and quantifying intrinsic tissue components and exogenous compounds, including fluorescent probes [17,25]. The herein developed combination of real-time epifluorescence and optoacoustic imaging offers important synergistic advantages. First, concurrent real-time validation with a well-established method is crucial for establishing accuracy and reproducibility of the OA imaging results. This is of particular importance for the visualization of rapid *in vivo* dynamics that cannot be reliably validated on an *ex vivo* specimen, e.g., in functional neuroimaging applications [26]. On the other hand, the higher resolution of optoacoustics in deep regions enables better localization of fluorescence agents in microvascular structures.

To the best of our knowledge, our proposed solution is the first to offer hybrid fluorescence-optoacoustic imaging of living tissues across large fields of view (FOVs) and real-time performance both in 2D and 3D. The implemented epifluorescence configuration is essential if the sample has limited accessibility, further facilitating image registration and enabling hand-held operation of the hybrid device to optimally support both pre-clinical and clinical studies. The specifically designed fiberscope used for fluorescence imaging enables covering a large ROI with high spatial and temporal resolution. The compact design of the fiberscope does not compromise the large angular detection coverage necessary for the accurate 3D OA image reconstruction. Light excitation for both modes is done with the same short-pulsed laser source, thus facilitating an effective registration and cross-validation of the images.

It was shown that the fiberscope provides optical imaging of superficial targets over a large spectral range with 44 μm spatial resolution and effective FOV of ~80 mm^2. The resolution slightly deteriorates for NIR wavelengths due to crosstalk between the individual fibers; yet, it matches well the ~175 μm spatial resolution of the optoacoustic system. As a practical example, it was shown that the cortical microvasculature of the mouse brain could be resolved with epifluorescence after scalp removal and contrast enhancement by a fluorescent agent. On the other hand, OA allowed volumetric imaging of the deep brain without deterioration of the spatial resolution with depth. It should be noted that higher spatial resolution can be achieved with nearly the same OA system by using a spherical array with a larger detection bandwidth which, however, comes at the expense of a smaller effective FOV. The real-time 3D imaging capacity of OA also makes it more suitable for monitoring the dynamics of injected contrast agents, even for superficial regions.

In conclusion, the newly developed hybrid system enabled, for the first time, to the best of our knowledge, registered real-time epifluorescence and 4D OA imaging, making it especially useful for accurate monitoring of fluorescence-based signal dynamics in highly scattering samples. The proposed synergistic combination and cross-validation between fluorescence and optoacoustic imaging can benefit numerous studies looking at multi-scale *in vivo* dynamics, such as functional neuroimaging, visualization of organ perfusion and contrast agent uptake, cell tracking, and pharmacokinetic and bio-distribution analysis.

Funding. H2020 European Research Council (ERC) (ERC-2015-CoG-682379); National Institute of Health (R21-EY026382); Human Frontier Science Program (HFSP) (RGY0070/2016); Deutsche Forschungsgemeinschaft (DFG) (RA1848/5-1).

Acknowledgment. The authors would like to thank M. Reiss and U. Klemm for their assistance in animal experimentation.

REFERENCES

1. J. W. Lichtman and J. Conchello, Nat. Methods **2**, 910 (2005).
2. Editorial, Nat. Photonics **3**, 361 (2009).
3. L. Tian, S. A. Hires, T. Mao, D. Huber, M. E. Chiappe, S. H. Chalasani, L. Petreanu, J. Akerboom, S. A. McKinney, E. R. Schreiter, C. I. Bargmann, V. Jayaraman, K. Svoboda, and L. L. Looger, Nat. Methods **6**, 875 (2009).
4. K. Pu, A. J. Shuhendler, J. V. Jokerst, J. Mei, S. S. Gambhir, Z. Bao, and J. Rao, Nat. Nanotechnol. **9**, 233 (2014).
5. M. de Jong, J. Essers, and W. M. van Weerden, Nat. Rev. Cancer **14**, 481 (2014).
6. A. Ale, V. Ermolayev, E. Herzog, C. Cohrs, M. H. de Angelis, and V. Ntziachristos, Nat. Methods **9**, 615 (2012).
7. Y. Ma, M. A. Shaik, M. G. Kozberg, S. H. Kim, J. P. Portes, D. Timerman, and E. M. C. Hillman, Proc. Natl. Acad. Sci. USA **113**, E8463 (2016).
8. Y. Gong, C. Huang, J. Z. Li, B. F. Grewe, Y. Zhang, S. Eismann, and M. J. Schnitzer, Science **350**, 1361 (2015).
9. G. Hong, S. Diao, J. Chang, A. L. Antaris, C. Chen, B. Zhang, S. Zhao, D. N. Atochin, P. L. Huang, K. I. Andreasson, C. J. Kuo, and H. Dai, Nat. Photonics **8**, 723 (2014).
10. X. L. Deán-Ben and D. Razansky, Opt. Express **21**, 28062 (2013).
11. D. Razansky, A. Buehler, and V. Ntziachristos, Nat. Protocols **6**, 1121 (2011).
12. D. Razansky, M. Distel, C. Vinegoni, R. Ma, and N. Perrimon, Nat. Photonics **3**, 412 (2009).
13. D. Razansky, J. Baeten, and V. Ntziachristos, Med. Phys. **36**, 939 (2009).
14. X. L. Deán-Ben and D. Razansky, Light: Sci. Appl. **3**, e137 (2014).
15. J. Weber, P. C. Beard, and S. E. Bohndiek, Nat. Methods **13**, 639 (2016).
16. I. Stoffels, S. Morscher, I. Helfrich, U. Hillen, J. Leyh, N. C. Burton, T. C. Sardella, J. Claussen, T. D. Poeppel, H. S. Bachmann, A. Roesch, K. Griewank, D. Schadendorf, M. Gunzer, and J. Klode, Sci. Transl. Med. **7**, 317ra199 (2015).
17. X. L. Deán-Ben, S. Gottschalk, L. B. Mc, S. Shoham, and D. Razansky, Chem. Soc. Rev. **46**, 2158 (2017).
18. B. Wang, Q. Zhao, N. M. Barkey, D. L. Morse, and H. Jiang, Med. Phys. **39**, 2512 (2012).
19. C. Kim, K. H. Song, F. Gao, and L. V. Wang, Radiology **255**, 442 (2010).
20. I. Kosik and J. J. L. Carson, Proc. SPIE **8581**, 858143 (2013).
21. Y. Wang, K. Maslov, C. Kim, S. Hu, and L. V. Wang, IEEE Trans. Biomed. Eng. **57**, 2576 (2010).
22. B. Rao, F. Soto, D. Kerschensteiner, and L. V. Wang, J. Biomed. Opt. **19**, 36002 (2014).
23. X. L. Deán-Ben and D. Razansky, Photoacoustics **4**, 133 (2016).
24. M. Xu and L. V. Wang, Phys. Rev. E **71**, 16706 (2005).
25. X. L. Deán-Ben and D. Razansky, Photoacoustics **1**, 68 (2013).
26. X. L. Deán-Ben, G. Sela, A. Lauri, M. Kneipp, V. Ntziachristos, G. Westmeyer, S. Shoham, and D. Razansky, Light: Sci. Appl. **5**, e16201 (2016).